Accepted Manuscript

DNA mismatch repair proteins MLH1 and PMS2 can be imported to the nucleus by a classical nuclear import pathway

Andrea C. de Barros, Agnes A.S. Takeda, Thiago R. Dreyer, Adrian Velazquez-Campoy, Boštjan Kobe, Marcos R.M. Fontes

Please cite this article as: Keplinger M, Marhofer P, Moriggl B, Zeitlinger M, Muehleder-Matterey S, Marhofer D, Cutaneous innervation of the hand: clinical testing in volunteers shows that variability is far greater than claimed in textbooks, *British Journal of Anaesthesia* (2017), doi: 10.1016/j.bja.2017.09.008.

ABSTRACT

MLH1 and PMS2 proteins form the MutLα heterodimer, which plays a major role in DNA mismatch repair (MMR) in humans. Mutations in MMR-related proteins are associated with cancer, especially with colon cancer. The N-terminal region of MutLα comprises the N-termini of PMS2 and MLH1 and, similarly, the C-terminal region of MutLα is composed by the C-termini of PMS2 and MLH1, and the two are connected by linker region. The nuclear localization sequences (NLSs) necessary for the nuclear transport of the two proteins are found in this linker region. However, the exact NLS sequences have been controversial, with different sequences reported, particularly for MLH1. The individual components are not imported efficiently, presumably due to their C-termini masking their NLSs. In order to gain insights into the nuclear transport of these proteins, we solved the crystal structures of importin-α bound to peptides corresponding to the supposed NLSs of MLH1 and PMS2 and performed isothermal titration calorimetry to study their binding affinities. Both putative MLH1 and PMS2 NLSs can bind to importin-α as monopartite NLSs, which is in agreement with some previous studies. However, MLH1-NLS has the highest affinity already measured by a natural NLS peptide, suggesting a major role of MLH1 protein in nuclear import compared to PMS2. Finally, the role of MLH1 and PMS2 in the nuclear transport of the MutLα heterodimer is discussed.

DNA Mismatch Repair Proteins MLH1 and PMS2 Can Be Imported to the Nucleus by a Classical Nuclear Import Pathway

Andrea C. de Barros[a], Agnes A. S. Takeda[a], Thiago R. Dreyer[a], Adrian Velazquez-Campoy[b], Boštjan Kobe[c] and Marcos R. M. Fontes[a*]

[a]Departamento de Física e Biofísica, Instituto de Biociências, Universidade Estadual Paulista, Botucatu, SP, Brazil

[b]Institute of Biocomputation and Physics of Complex Systems (BIFI), Joint-Unit IQFR-CSIC-BIFI, and Dep. of Biochemistry and Molecular and Cell Biology, University of Zaragoza, Zaragoza, Spain, and Fundacion ARAID, Government of Aragon, Zaragoza, Spain.

[c]School of Chemistry and Molecular Biosciences, Institute for Molecular Bioscience and Australian Infectious Diseases Research Centre, University of Queensland, Brisbane, Queensland 4072, Australia

[*]To whom correspondence should be addressed: Marcos R. M. Fontes, Departamento de Física e Biofísica, Instituto de Biociências, Universidade Estadual Paulista, Botucatu, SP, 18618-970, Brazil; E-mail: fontes@ibb.unesp.br; Fax: +55-14-38153744; Phone: +55-14-38800271.

Abstract

MLH1 and PMS2 proteins form the MutLα heterodimer, which plays a major role in DNA mismatch repair (MMR) in humans. Mutations in MMR-related proteins are associated with cancer, especially with colon cancer. The N-terminal region of MutLα comprises the N-termini of PMS2 and MLH1 and, similarly, the C-terminal region of MutLα is composed by the C-termini of PMS2 and MLH1, and the two are connected by linker region. The nuclear localization sequences (NLSs) necessary for the nuclear transport of the two proteins are found in this linker region. However, the exact NLS sequences have been controversial, with different sequences reported, particularly for MLH1. The individual components are not imported efficiently, presumably due to their C-termini masking their NLSs. In order to gain insights into the nuclear transport of these proteins, we solved the crystal structures of importin-α bound to peptides corresponding to the supposed NLSs of MLH1 and PMS2 and performed isothermal titration calorimetry to study their binding affinities. Both putative MLH1 and PMS2 NLSs can bind to importin-α as monopartite NLSs, which is in agreement with some previous studies. However, MLH1-NLS has the highest affinity already measured by a natural NLS peptide, suggesting a major role of MLH1 protein in nuclear import compared to PMS2. Finally, the role of MLH1 and PMS2 in the nuclear transport of the MutLα heterodimer is discussed.

1. Introduction

The maintenance of the genome integrity and stability is important to ensure the organisms survival as well as the accurate transmission of the genetic code. The DNA repair machineries are highly conserved across species from bacteria to humans [1, 2]. The DNA mismatch repair (MMR) system is responsible for recognizing and repairing mismatched base pairs generated during DNA replication [3, 4], for removing base mismatches caused by spontaneous or induced base deamination, oxidation, methylation, replication errors, and also for activating cell death when DNA repair fails [2, 5]. The inactivation of MMR in human cells is associated with hereditary and sporadic human cancers [6], but particularly with hereditary nonpolyposis colon cancer [7, 8].

The MMR system is best characterized in *Escherichia coli* and comprises the MutS, MutL and MutH protein complexes [9]. The MutS homodimer identifies DNA mismatches and mobilizes the homodimer MutL to perform DNA repairs. This homodimer activates the endonuclease MutH, which recognizes the newly synthesized strand by the lack of methylation, promotes the strand cleavage and initiates repair by introduction of an entry-point for the excision reaction. The activity of helicases, exonucleases, DNA polymerase III and ligase completes the repair [1, 10]. Other organisms have MutS and MutL homologues, playing the same initial steps, however the functions were split between heterodimeric proteins [11]. The human MutS homologue MutSα heterodimer (MSH2/MSH6 proteins) recognizes the new strand due the base-base mismatches, while MutSβ heterodimer (MSH2/MSH3 proteins) recognizes primarily longer insertions and deletions [11]. Then, the human MutL homologue MutLα heterodimer (MLH1/PMS2 proteins) promotes the incision of the discontinuous strand, followed by exonuclease1 (EXO1) activity [1, 2]. The segment containing the mismatch is removed and the repair can be completed.

MLH1 and PMS2 proteins form MutLα heterodimer that is essential for human MMR [1-3, 9, 10]. The N-terminal region of MutLα comprises the N-termini of PMS2 and MLH1 and, similarly, the C-terminal region of MutLα is composed by the C-termini of PMS2 and MLH1, and the two are connected by linker region that provide flexibility to the heterodimer. PMS2 also displays a metal-binding motif in its C-terminal region that is essential for the endonuclease activity of MutLα. The putative nuclear localization sequences (NLSs) are found in the linker regions of both PMS2 and MLH1 [2, 3, 12]. Several DNA repair proteins [4] are imported into the nucleus using the classical import pathway, in which importin-α (Impα) recognizes a NLS present in the cargo protein [13]. The classical NLS corresponds to one or two clusters of basic amino acid residues, defined as monopartite and bipartite, whose consensus correspond to K(K/R)X(K/R) and $KRX_{10-12}K(K/R)X(K/R)$ (where X corresponds to any residue), respectively. These sequences bind to Impα through hydrophobic and polar contacts with two binding sites, known as major and minor binding sites. Bipartite NLSs have interactions with both binding sites, while monopartite NLSs bind preferentially to the major site [14-17]. The importin-β (Impβ) carrier binds to Impα adaptor and the heterotrimer (Impα/Impβ/cargo protein) is translocated to the nucleus through interactions between Impβ and the nucleoporins from the nuclear pore complex [18-20]. The release of cargo proteins is also dependent of nucleoporins (e.g., NUP50) [13, 19, 21], RanGTP and other regulatory proteins, and Impα and Impβ are recycled for a new import cycle [22].

The nuclear import of DNA repair proteins by the classical pathway has been reported as an important feature that regulates the interdependence of these proteins in the DNA repair processes [2, 4, 23]. A previous study of Wu and colleagues [2] indicated that specific NLSs of MLH1 and PMS2 located in their linker regions need to be unmasked by the C-termini of these proteins to allow an efficient nuclear import. A second study evaluated several NLS mutants by immunofluorescence microscopy and confirmed the previous proposed

monopartite NLSs of the MutLα heterodimer [3]. More recently, a third study proposed that different NLSs for MLH1 (bipartite NLS) and PMS2 (monopartite NLS) are responsible for their translocation to the nucleus [24]. Thus, in order to provide insights about the structural basis of the protein import mechanism of MutLα proteins, herein we performed a crystallographic study with putative NLS peptides of MLH1 and PMS2 (including native and mutated ones) complexed to Impα and quantified the interactions of the peptides with Impα using isothermal titration calorimetry (ITC) assays.

2. Material and Methods

2.1. Synthesis of NLS peptides

The peptides corresponding to human MLH1 NLS ([466]SSNPRKRHRED[476]), and their respective mutants MLH1-K471N ([466]SSNPRNRHRED[476]), MLH1-R472N ([466]SSNPRKNHRED[476]), human PMS2 NLS ([571]LATPNTKRFKKEE[583]), and mutants PMS2-K577N ([571]LATPNTNRFKKEE[583]), PMS2-R578N ([571]LATPNTKNFKKEE[583]) were synthesized by Proteimax (Brazil) with purity higher than 99%. The peptides proposed by Leong and co-workers [24] for MLH1 ([459]SEKRGPTSSNPRKRHRED[476]) and PMS2 ([625]LAKRIKQL[632]) (referred herein as MLH1L and PMS2L, respectively) were also synthesized by the same company with purity higher than 99%. All peptides contain residues at their N- and C-termini additional to minimal identified NLS [4], to avoid artifactual binding modes at the termini [14] (Table 1).

2.2. Protein expression and purification

Hexa-His-tagged N-terminally truncated *Mus musculus* importin-α2, composed of amino acids 70-529 (Impα), was expressed and purified by nickel affinity chromatography as described previously [25]. The protein was eluted using a gradient of imidazole, followed by dialysis. The Impα sample was stored in 20 mM Tris HCl pH 8.0, 100 mM sodium chloride, 10 mM DTT at -20 ºC. The purity was estimated to be 98% by SDS-PAGE.

2.3. Calorimetric assays

Binding affinities between the NLS peptides and Impα were determined by isothermal titration calorimetry (ITC). The experiments were carried out using a MicroCal iTC$_{200}$ microcalorimeter (GE Healthcare) at 20 °C. All samples were prepared in 20 mM Tris HCl, 100 mM NaCl (pH 8.0). The sample cell was loaded with Impα (30 µM) that was individually titrated with each of the NLS peptides. Twenty successive injections (2 µL) of NLS peptides (SV40TAg (240 µM); MLH1 (450 µM), MLH1-K471N (600 µM), MLH1-R472N (600 µM); PMS2 (240 µM), PMS2-K577N (450, 750 and 15000 µM), PMS2-R578N (240 and 450 µM), MLH1L (450 µM) and PMS2L (300 µM)) were carried out into the calorimetric cell, in an interval of 240 s for each titration and 800-rpm homogenization speed. The thermodynamic parameters dissociation constant (K_d) and enthalpy change (ΔH) were obtained by fitting the binding isotherm data as previously proposed [26]. Titrations were performed in triplicate and the heat dilution of each peptide was determined from control experiments and subtracted from their binding titrations prior to data analysis.

2.4. Crystallization and crystal structure determination

Impα was concentrated to 18 mg/mL using a Vivaspin 20, 30 kDa (GE Healthcare) and stored at -20 °C. Peptides was prepared with the concentration of 16 and 19 mg/mL for MLH1 and PMS2 NLS, respectively. Crystallization conditions were screened using, as a starting point, the conditions that had been successful for other peptide complexes [14, 27]. The crystals were obtained using co-crystallization, by combining 1 μl of protein solution, 0.5 μl of peptide solution (peptide/protein molar ratio of 8), and 1 μl of reservoir solution on a coverslip, and suspending the mixture over 0.5 ml of reservoir solution. Single crystals were obtained with reservoir solutions containing 0.600-0.625 M sodium citrate (pH 6) and 10 mM DTT after 15-20 days. The Impα complexes with mutated peptides MLH1-K471N, MLH1-R472N, PMS2-K577N and PMS2-R578N did not result in crystals.

X-ray diffraction data were collected from a single crystal at Laboratório Nacional de Luz Síncrotron (LNLS), Campinas, Brazil, with a MarMosaic 225 detector (MAR Research) at the beamline MX-2. The crystals were mounted in nylon loops, transiently soaked in a reservoir solution supplemented with 25% glycerol and flash-cooled at 100 K in a nitrogen stream (Oxford Nitrogen Cryojet XL- Oxford Cryosystems). Data were processed using the HKL2000 package [28]. The crystals had the symmetry of the space group $P2_12_12_1$ and were isomorphous to other Impα-NLS peptide complexes (Table 2). The structure of the complex with CN-SV40TAg NLS (extended SV40TAg NLS peptide, comprising TAg amino acids 110–132; PDB ID 1Q1S[29]), with the NLS peptides omitted, was employed as the starting model for crystallographic refinement. After rigid body refinement, programs Refmac5 [30] and Phenix [31] were used to refine the structures and the program Coot [32] was used for manual modeling. The final model of the Impα:MLH1 NLS complex consists of 424 residues of Impα (71-497), 2 peptide ligands (10 residues could be modeled in the major site and 9 residues could be modeled in the minor site), 225 water molecules and 1 DTT molecule, while the final model of the Impα:PMS2 NLS complex consists of 424 residues of Impα (71-

497), 1 peptide ligand (11 residues could be modeled in the major site), 332 water molecules and 1 DTT molecule (Table 2). Stereochemistry of the structure was evaluated with the program PROCHECK [33] and the contacts were analyzed using the program LIGPLOT [34] (Table 2). Coordinates and structure factors have been deposited in the PDB under accession code 5U5P (Impα-MLH1 NLS) and 5U5R (Impα-PMS2 NLS).

3. Results

3.1. Structure of Impα in complex with peptides corresponding to MLH1 and PMS2 NLSs

The N-terminally truncated mouse Impα (Impα) was employed since it shares about 94% sequence identity and the NLS-binding sites are essentially identical to the human Impα [17] (Suppl. Fig. 1). It was co-crystallized with peptides corresponding to MLH1 and PMS2 NLSs as proposed previously [2,3] (Table 1). The co-crystals of wild-type NLSs were grown in similar conditions and were isomorphous to other mouse Impα crystals [14, 27]. The structures were refined at 2.17 and 2.10 Å resolution, respectively, for Impα-MLH1 NLS and Impα-PMS2 NLS complexes (Table 2). Electron density map of Impα-MLH1 NLS clearly showed electron density corresponding to the peptide in both the major and minor binding sites, while the Impα-PMS2 NLS complex showed electron density only in the major binding site (Fig. 1 and 2).

The superposition of the Impα structure in both the MLH1 and PMS2 NLS complexes with full-length Impα and other monopartite NLS peptide complexes [14, 23, 35] indicates that Impα structures are essentially identical to the structures reported previously. The root-mean-square deviations (RMSDs) of Cα atoms of Impα residues 72–496 are 0.35 and 0.33 Å between the full-length Impα (PDB ID 1IAL) and the Impα-MLH1 NLS or Impα-PMS2 NLS

complexes, respectively. The equivalent superposition between Impα-SV40TAg NLS (PDB ID 1EJL) and the Impα-MLH11 NLS or Impα-PMS2 NLS complexes yield RMSD values of 0.34 and 0.32Å, respectively.

3.2. Binding of MLH1 NLS to importin-α structure

The crystal structure of Impα-MLH1 NLS complex showed two separate volumes of electron density in the concave portion of Impα (Fig. 1A), corresponding to the MLH1 NLS peptides bound to the major and minor binding sites. The peptides could be modeled unambiguously in the electron density maps in antiparallel configuration when compared to the ARM repeats direction. The electron density found in the major NLS-binding site indicated the presence of 10 peptide residues (^{467}SNPR**KRHR**ED^{476}, where the boldface residues are bound to P_2-P_5 positions) with an average B-factor of 44.9 Å^2, which is similar to the average B-factor for entire Impα (45 Å^2) (Fig. 1B). The residues bound to the core of the major NLS-binding site (residues 470–474; positions P_1-P_5) have lower average B-factors (38.5 Å^2) compared to Impα. The residues R^{471} and K^{474} (positions P_2 and P_3 have the lowest B-factors (33.7 and 35.0 Å^2, respectively) and the largest number of interactions between NLS side-chains and side-chains of conserved residues of Impα (Fig. 3). The electron density found at the minor binding site corresponded to 9 peptide residues (^{467}SNPR**KR**HRE^{475}, where the boldface residues are bound to P_1' and P_2' positions) with average B-factor of 53.9 Å^2 (Fig. 1C). The residues bound to the core of the minor NLS-binding site (residues 471–474; positions P_1'- P_4') have slightly higher average B-factors (49.4 Å^2) compared to the entire protein. The buried surface area between the protein and the peptide corresponds to 814.1 Å^2 at the major site and 645.1 Å^2 at the minor site. The superposition of Cα atoms between

MLH1 and the simian virus 40 (SV40) large T-antigen (TAg) NLS peptides yields an RMSD of 0.10 Å for the major binding site and 0.35 Å for the minor binding site (Suppl. Fig. 2).

3.3. Binding of PMS2 NLS to importin-α structure

The crystal structure of Impα-PMS2 NLS complex shows unambiguously a single volume of electron density in the concave portion of Impα (Fig. 2A), corresponding to the PMS2 NLS peptide bound to the major binding site. Similar to MLH1 NLS, the peptide was modeled unambiguously in the electron density maps in an antiparallel configuration when compared to the ARM repeats direction. The electron density found in the major NLS-binding site indicated the presence of 11 peptide residues (^{573}TPNT**KRFK**KEE^{583}, where the boldface residues are bound to P_2-P_5 positions) with an average B-factor of 42.1 Å^2 (the average B-factor for Impα is 37.4 Å^2) (Fig. 2B). The residues bound to the core of the major NLS-binding site (576–580; positions P_1-P_5) have lower average B-factors (31.1 Å^2) compared to Impα. The residues K^{577} and K^{580} (positions P_2 and P_5) have the lowest B-factors (26.7 and 30.0 Å^2, respectively) and the largest number of interactions between NLS side-chains and side-chains of conserved residues of Impα (Fig. 3). The buried surface area between the protein and the peptide corresponds to 742.6 Å^2. The superposition of Cα atoms between PMS2 and SV40TAg NLS peptides yields an RMSD of 0.08 Å for the major binding site (Suppl. Fig. 1).

3.4. Calorimetric assays for the binding of NLS-peptides and Impα

ITC assays were used to quantify the interactions between Impα and the wild-type MLH1 NLS and two of its mutants (Table 1). Analogous experiments were performed with

PMS2 NLSs (Table 1). These mutants were chosen based on the crystal structures of Impα-PMS2 and MLH1 NLSs complexes and taking into account the consensus sequences for monopartite NLSs [15].

The MLH1-NLS isotherm profiles could be best fitted with a model of two non-identical and independent binding sites (Fig. 4). A dissociation constant was in the submicromolar range (~0.1 µM) and attributed to the major binding site, and the other constant corresponding to 15-fold lower affinity was attributed to the minor binding site (Table 3). Titrations of MLH1 NLS mutants (MLH1-K471N and MLH1-R472N) with Impα resulted in binding thermograms characteristic of non-interacting systems, not allowing the determination of thermodynamic parameters.

PMS2-NLS titration with Impα resulted in isotherm profiles indicating that PMS2 NLS binds only to the major binding site, consistent with crystallographic data, with moderate affinity (Fig. 4, Table 3). Similar to the MLH1 mutants assays, ITC experiments with PMS2-K577N and PMS2-R578N NLS peptides resulted in binding thermograms characteristic of non-interacting systems, not allowing the determination of thermodynamic parameters even when titrated with higher molar ratios compared to the wild-type peptide. No further considerations related to enthalpic behavior (Fig. 4) are commented here, since the enthalpy values may have predominant contributions from Tris buffer used in the assays, (it displays high ionization enthalpy) and, also, from polar ionizable amino acids of NLS-peptides.

A control ITC assay was performed with the peptide corresponding to SV40TAg NLS in order to compare its binding affinity to Impα in relation to the MLH1 and PMS2 NLSs, using the same experimental conditions (Fig. 4). The data was fitted with two non-identical and independent binding sites, based on the crystallographic data [14] and as previously proposed [36] (Table 3). The lower K_d value (higher affinity) was attributed to the binding of the SV40TAg NLS to major binding site of the Impα, which is in the same order of

magnitude compared to the PMS2 NLS, but one order of magnitude higher compared to the MLH1 NLS. The low-affinity K_d value, 10-fold higher than for the minor-site binding of the MLH1 NLS, was attributed to the binding of SV40TAg NLS to the minor binding site (Table 3).

In addition, to test the NLS peptides proposed by Leong and co-colleagues [24], ITC assays with the peptides MLH1L and PMS2L using the same experimental conditions of other peptides (Table 3). Titrations of MLH1L peptide with Impα resulted in binding thermograms characteristic of non-interacting systems, not allowing the determination of thermodynamic parameters (Suppl. Fig. 3A). To check if the observed results were related to binding with a zero enthalpic change, we also performed the same experiments, but using a lower temperature (10 $^{\circ}$C). Indeed, the result of this assays demonstrated a non-binding interaction system (Suppl. Fig. 3B). Previous ITC binding studies [37] showed that if interaction between ligand and protein is observed, a non-zero enthalpic change would be noticed due to the non-zero heat capacity. In contrast, PMS2L titration with Impα resulted in isotherm profiles that could be best fitted with a model of two non-identical and independent binding sites (Fig. 4, Table 3). A dissociation constant was in the submicromolar range, being attributed to the major binding site, and the second constant present lower affinity (17-fold lower affinity) was attributed to the minor binding site (Table 3).

4. DISCUSSION

4.1. MLH1 and PMS2 have classical monopartite NLSs

Two amino-acid sequences of MLH1 (^{466}SSNP**RKRHR**ED^{476} where the boldface residues are bound to P_2-P_5 positions) and PMS2 (^{571}LATPNT**KRFK**KEE^{583}) proteins were

identified as the minimum region required for nuclear import [2, 3]. Controversially, another study [24] suggested a bipartite sequence for MLH1 with a linker region of only 8 residues ([459]SE**KR**GPTSSNP**RKRHR**ED[476], where the boldface residues are bound to P_1'-P_2' and P_2-P_5 positions), and a different monopartite sequence for the PMS2 containing similar key residues ([625]LA**KRIK**QL[632]). The proposal of a linker region with only 8 residues for MLH1 is inconsistent with a number of studies that have demonstrated that the linker region of bipartite NLSs should have a minimum length of 10 residues, otherwise it would be structurally impossible for the peptide to bind in both minor and major sites of the Impα simultaneously [17, 24, 38, 39]. In the case of the PMS2, both the proposed NLSs should be able to bind to Impα because they have the same key residues conserved (KRXK), which are able to bind at positions P_2, P_3, and P_5, consistent with the monopartite NLS consensus K(K/R)X(K/R). Interesting, ITC assays (section 3.4) with the peptides proposed by Leong and co-workers (MLH1L and PMS2L) [24] showed that MLH1L does not bind to Impα with detectable affinity and PMS2L binds to Impα with similar values compared to other monopartite NLS peptides (Table 3). As expected, MLH1L peptide did not bind to Impα as a classical bipartite NLS, but why this peptide did not bind to the major binding site is unclear and need further investigations. On the other hand, PMS2L binds to Impα as a classical monopartite NLS, thus this sequence is a possible NLS of the PMS2 protein.

In order to study the structural determinants of binding between the NLS peptides proposed for MLH1 and PMS2 and Impα [2, 3], we performed co-crystallization and solved the crystal structures of the Impα-MLH1 NLS and Impα-PMS2 NLS complexes. The crystal structure of the Impα-MLH1 NLS complex contains the MLH1 NLS peptide interacting at two binding sites. The residues K^{471}, R^{472} and R^{474} bind at positions P_2, P_3, and P_5, respectively, of the major binding site. These data are in agreement with the monopartite NLS consensus K(K/R)X(K/R) [15]. The contacts of the peptide with the minor binding site

include residues K^{471}, R^{472}, which bind at positions P_1' and P_2', respectively. The binding of monopartite NLSs at the Impα minor site is observed for several complexes [14, 35, 40, 41], particularly those that contain KR sequence [35, 40-42]. Structural comparisons of the MLH1 NLS peptide, with the classical monopartite NLS peptides, such as SV40TAg NLS [14], Ku70, Ku80 [23], XPG1 and XPG2 NLSs [35], show that these structures are well conserved, as observed in Suppl. Fig. 1. In contrast to the complex with MLH1 NLS peptide, the crystal structure of the Impα-PMS2 NLS complex shows the peptide interacting only with the major binding site of the protein. This fact is probably related to the low content of K/R residues that would bind at the positions P_0'-P_4' for the PMS2 NLS, decreasing its affinity to this site (refer to the section 4.3). This feature is not usual for the majority for Impα-monopartite NLSs, but it was already observed for other NLS complexes, particularly the NLS from the DNA repair proteins (Ku70 and Ku80 [23]). The residues K^{577}, K^{578} and K^{580} of the PMS2 bind at positions P_2, P_3, and P_5, which is also consistent to the classical monopartite NLS consensus. Structural comparisons of the PMS2 peptide with classical NLS monopartite peptides shows that PMS2 NLS structure establishes analogous contacts observed for other NLSs (Suppl. Fig. 1). Similar to the co-crystallization experiments with MLH1 NLS mutants, PMS2 NLS mutants PMS2-K577N and PMS2-R578N and Impα did not yield any crystals, which may also be attributed to the lack of interaction between the peptides and the protein.

4.2. A comparison between binding affinities of NLSs and Impα by ITC

Affinity assays are fundamental to obtain a quantitative description of structure recognition and to determine the potency of a protein-NLS binding. Several studies have measured the affinity and identify the binding behavior between NLSs and Impα, using different methodologies, such as solid-state binding assays, surface plasmon resonance and

ITC; the latter has been most widely used [23, 35, 36, 38, 39, 42-50]. However, a systematic affinity comparison is only possible when using the same technique, and similar conditions (e.g. temperature and buffer) and ideally the same equipment (e.g. ITC_{200}, VP-ITC, Affinity ITC, Nano ITC). ITC assays using different NLS peptides and Impα from different families revealed dissociated constants varying from hundreds of nanomolar ($K_d \sim 0.1$ µM) to approximately 50 µM for the major NLS binding site. Interestingly, MLH1 NLS presents the highest affinity already measured using ITC assays and PMS2 is among the weakest natural NLSs to bind Impα at the major binding site (Table 3). PMS2 NLS displays similar affinity compared to the most studied monopartite NLS, SV40TAg NLS, ~2 µM (present study, [36, 47]) using a microcalorimeter. Interestingly, XPG NLS peptides, which also have a combination of K/R residues at the positions P_1-P_5 (Table 4), have K_d values between 0.4-0.9 µM [23].

On the other hand, monopartite NLS peptides usually have affinities for the minor binding site one order of magnitude lower compared to the major site ($K_d \sim 1$-10 µM). Interestingly, MLH1 NLS also displays a very high affinity for this site and PMS2 has no detectable affinity for this site. NLS peptides that bind with low affinities to this site have been observed using ITC assays (e.g. hPLSCR [45], $K_d = 48.7$ µM; XPG2 [35], $K_d = 140$ µM). In contrast, for Impα from the α1 family (rice [46] and filamentous fungus [47]), the affinity of NLS peptides to the minor binding site is similar for the major binding site [47], or even stronger [46].

The importance of particular interactions, such as those highlighted by MLH1-K471N, MLH1-R472N, PMS2-K577N and PMS2-R578N peptides, in which key residues of the positions P_2 or P_3 were mutated, can be easily characterized using the ITC technique. These data confirm previous results regarding to minimum consensus sequences for NLSs [15]. However, for both MLH1 and PMS2, Brieger and colleagues [3] observed some low-level

localization of the NLS mutants into the cell nuclei. This suggests that these mutants, despite having low affinity for Impα not detectable by ITC, may still support some low level of nuclear import [45].

Taking into account both structural and calorimetric data of several NLS/Impα complexes, it is possible to get clues about the most favorable interactions between NLSs and the receptor. For example, in addition to P_2 and P_5 positions, P_3 is the most important one, but it is not mandatory, as TXP2 NLS [51] has a Met in this position. However, from Tables 3 and 4, it is possible to hypothesize that an Arg residue is more favorable than Lys in the position P_3, because it is frequent in the NLSs with high affinity, e.g. MLH1 and XPG1. Charged residues, such as Glu and Asp at the C-termini and Ser in the N-termini, also seem to be favorable (Tables 3 and 4). Both observations are also seen in optimized bipartite NLS sequences Bimax1 and Bimax2 [14-17].

4.3. The functional role of MLH1 and PMS2 in nuclear transport

Wu and colleagues [2] demonstrated that isolated PMS2 protein is not detected in the nucleus for the majority of cells used in their experiments (95 %). In contrast, the same experiment with MLH1 resulted in 51 % of cells with the protein located only in the cytoplasm and the remain 49 % of cells present the protein fractioned between cytoplasm and nucleus. Interestingly, C-terminally truncated MLH1 and PMS2 proteins that retain their proposed NLSs are localized in the nucleus, but C-terminally truncated MLH1 and PMS2 proteins that lack the putative NLSs are localized exclusively in the cytoplasm [2]. Taking into account these results, the authors of this study suggested that C-terminal regions of these proteins mask their NLSs, impairing their nuclear transport. Thus, when the MLH1/PMS2 complex is formed, NLSs are exposed and the heterodimer can be transported to the nucleus.

In addition, these authors also hypothesized that the competition for dimer formation of the MLH1 with other proteins, such as PMS1 and MLH3, rather than PMS2, is a regulatory mechanism for an adaptive response during DNA repair. The results presented here are in agreement with the results and hypotheses of Wu and colleagues [2] and other studies [3, 52], where NLSs from both proteins are able to bind Impα, but the MLH1 NLS plays a major role. Indeed, we demonstrated that the MLH1 NLS has a very high affinity to Impα compared to other proteins (Table 3) and, particularly compared to the PMS2 NLS.

Using confocal laser microscopy, Brieger and colleagues [3] performed an extensive analysis of two possible NLSs for MLH1 and 11 different mutants of these sequences; furthermore, they also studied one NLS sequence for PMS2 and 6 different mutants. The results obtained here are in total agreement with this study, in which the proposed NLS for MLH1 was able to bind Impα with very high affinity, an order of magnitude higher compared to the classical SV40TAg NLS [14]. Furthermore, the NLS mutants MLH1-K471N and MLH1-R472N, which were found predominantly localized in the cytoplasm by Brieger and colleagues [3], showed no detectable affinity to Impα by ITC assays. Similarly, we also confirmed that the proposed sequence for PMS2 was able to bind Impα and its mutants K577N and R578N were unable to bind to Impα with detectable affinity.

Finally, one question remains to be the answered: if just one NLS is enough to transport the MLH1/PMS2, why both proteins contain NLSs? Considering the affinity results obtained here and also the more efficient transport of the full-length MLH1 compared to PMS2 [2], we suggest that MLH1 plays the major role in the nuclear transport of MutLα (MLH1/ PMS2) complex. In addition, as MLH1 dimerizes with other partners (e.g. PMS1 and MLH3) to form other MutL complexes, its role in the import process of other complexes [2, 53, 54] is also probable. Possible explanations for the presence of NLS in PMS2 may include: (i) the observed basic sequences of residues for PMS2 is not functionally used for import

processes; (ii) redundancy of the NLSs to guarantee the nuclear transport of the MutLα, as suggested by Leong and colleagues [24]; (iii) PMS2 may be involved in other important processes related to other complexes, although such processes have not been observed yet; and (iv) different affinities may be related to regulation of the import of DNA repair proteins.

Although it is not possible to answer this question at this moment, similar results were also obtained by us for the Ku complex (Ku70/Ku80), which is involved in the non-homologous end-joining pathway of DNA repair. Both Ku70 and Ku80 proteins have NLSs, but the affinity of the Ku70 protein for Impα is 4-fold stronger, compared to Ku80 [23]. Consequently, we hypothesized that the presence of NLSs with different affinities may be related to regulation of nuclear transport of DNA repair proteins, which can also use Impα from different families as a fine adjustment.

In conclusion, we showed that both MLH1 and PMS2 NLSs proposed by two independent studies [2, 3] can bind to Impα as classical monopartite NLSs. Furthermore, we demonstrated that MLH1 NLS has the highest affinity already measured by ITC of a natural NLS peptide and, probably, plays a major role in the nuclear import of the MutLα heterodimer. On basis of previous and the present studies we obtained new insights into the binding specificities for NLS peptides to the minor binding site.

FUNDING

REFERENCES

[1] K. Fukui, DNA mismatch repair in eukaryotes and bacteria, J Nucleic Acids, 2010 (2010).

[2] X. Wu, J.L. Platt, M. Cascalho, Dimerization of MLH1 and PMS2 limits nuclear localization of MutLalpha, Mol Cell Biol, 23 (2003) 3320-3328.

[3] A. Brieger, G. Plotz, J. Raedle, N. Weber, W. Baum, W.F. Caspary, S. Zeuzem, J. Trojan, Characterization of the nuclear import of human MutLalpha, Mol Carcinog, 43 (2005) 51-58.

[4] N.O. Knudsen, S.D. Andersen, A. Lutzen, F.C. Nielsen, L.J. Rasmussen, Nuclear translocation contributes to regulation of DNA excision repair activities, DNA Repair (Amst), 8 (2009) 682-689.

[5] M. Christmann, M.T. Tomicic, W.P. Roos, B. Kaina, Mechanisms of human DNA repair: an update, Toxicology, 193 (2003) 3-34.

[6] G.M. Li, Mechanisms and functions of DNA mismatch repair, Cell Res, 18 (2008) 85-98.

[7] P. Peltomaki, DNA mismatch repair and cancer, Mutat Res, 488 (2001) 77-85.

[8] P. Peltomaki, H.F. Vasen, Mutations predisposing to hereditary nonpolyposis colorectal cancer: database and results of a collaborative study. The International Collaborative Group on Hereditary Nonpolyposis Colorectal Cancer, Gastroenterology, 113 (1997) 1146-1158.

[9] P. Modrich, Mechanisms in E. coli and Human Mismatch Repair (Nobel Lecture), Angew Chem Int Ed Engl, 55 (2016) 8490-8501.

[10] F.S. Groothuizen, T.K. Sixma, The conserved molecular machinery in DNA mismatch repair enzyme structures, DNA Repair (Amst), 38 (2016) 14-23.

[11] F.S. Groothuizen, T.K. Sixma, The conserved molecular machinery in DNA mismatch repair enzyme structures, DNA repair, 38 (2016) 14-23.

[12] E. Gueneau, C. Dherin, P. Legrand, C. Tellier-Lebegue, B. Gilquin, P. Bonnesoeur, F. Londino, C. Quemener, M.H. Le Du, J.A. Marquez, M. Moutiez, M. Gondry, S. Boiteux, J.B. Charbonnier, Structure of the MutLalpha C-terminal domain reveals how Mlh1 contributes to Pms1 endonuclease site, Nat Struct Mol Biol, 20 (2013) 461-468.

[13] M. Christie, C.W. Chang, G. Rona, K.M. Smith, A.G. Stewart, A.A. Takeda, M.R. Fontes, M. Stewart, B.G. Vertessy, J.K. Forwood, B. Kobe, Structural Biology and Regulation of Protein Import into the Nucleus, J Mol Biol, 428 (2016) 2060-2090.

[14] M.R. Fontes, T. Teh, B. Kobe, Structural basis of recognition of monopartite and bipartite nuclear localization sequences by mammalian importin-alpha, J Mol Biol, 297 (2000) 1183-1194.

[15] D. Chelsky, R. Ralph, G. Jonak, Sequence requirements for synthetic peptide-mediated translocation to the nucleus, Mol Cell Biol, 9 (1989) 2487-2492.

[16] M. Marfori, A. Mynott, J.J. Ellis, A.M. Mehdi, N.F. Saunders, P.M. Curmi, J.K. Forwood, M. Boden, B. Kobe, Molecular basis for specificity of nuclear import and prediction of nuclear localization, Biochim Biophys Acta, 1813 (2011) 1562-1577.

[17] M. Marfori, T.G. Lonhienne, J.K. Forwood, B. Kobe, Structural basis of high-affinity nuclear localization signal interactions with importin-alpha, Traffic, 13 (2012) 532-548.

[18] M. Stewart, Molecular mechanism of the nuclear protein import cycle, Nat Rev Mol Cell Biol, 8 (2007) 195-208.

[19] M. Stewart, Structural basis for the nuclear protein import cycle, Biochem Soc Trans, 34 (2006) 701-704.

[20] A. Cook, F. Bono, M. Jinek, E. Conti, Structural biology of nucleocytoplasmic transport, Annu Rev Biochem, 76 (2007) 647-671.

[21] Y. Matsuura, M. Stewart, Nup50/Npap60 function in nuclear protein import complex disassembly and importin recycling, EMBO J, 24 (2005) 3681-3689.

[22] S.J. Lee, Y. Matsuura, S.M. Liu, M. Stewart, Structural basis for nuclear import complex dissociation by RanGTP, Nature, 435 (2005) 693-696.

[23] A.A. Takeda, A.C. de Barros, C.W. Chang, B. Kobe, M.R. Fontes, Structural basis of importin-alpha-mediated nuclear transport for Ku70 and Ku80, J Mol Biol, 412 (2011) 226-234.

[24] V. Leong, J. Lorenowicz, N. Kozij, A. Guarne, Nuclear import of human MLH1, PMS2, and MutLalpha: redundancy is the key, Mol Carcinog, 48 (2009) 742-750.

[25] T. Teh, T. Tiganis, B. Kobe, Crystallization of importin alpha, the nuclear-import receptor, Acta Crystallogr D Biol Crystallogr, 55 (1999) 561-563.

[26] S. Vega, O. Abian, A. Velazquez-Campoy, A unified framework based on the binding polynomial for characterizing biological systems by isothermal titration calorimetry, Methods, 76 (2015) 99-115.

[27] M.R. Fontes, T. Teh, D. Jans, R.I. Brinkworth, B. Kobe, Structural basis for the specificity of bipartite nuclear localization sequence binding by importin-alpha, J Biol Chem, 278 (2003) 27981-27987.

[28] Z. Otwinowski, W. Minor, et al., Processing of X-ray diffraction data collected in oscillation mode, Methods Enzymol, 276 (1997) 307-326.

[29] M.R. Fontes, T. Teh, G. Toth, A. John, I. Pavo, D.A. Jans, B. Kobe, Role of flanking sequences and phosphorylation in the recognition of the simian-virus-40 large T-antigen nuclear localization sequences by importin-alpha, Biochem J, 375 (2003) 339-349.

[30] G.N. Murshudov, A.A. Vagin, E.J. Dodson, Refinement of macromolecular structures by the maximum-likelihood method, Acta Crystallogr D Biol Crystallogr, 53 (1997) 240-255.

[31] P.D. Adams, R.W. Grosse-Kunstleve, L.W. Hung, T.R. Ioerger, A.J. McCoy, N.W. Moriarty, R.J. Read, J.C. Sacchettini, N.K. Sauter, T.C. Terwilliger, PHENIX: building new software for automated crystallographic structure determination, Acta Crystallogr D Biol Crystallogr, 58 (2002) 1948-1954.

[32] P. Emsley, K. Cowtan, Coot: model-building tools for molecular graphics, Acta Crystallogr D Biol Crystallogr, 60 (2004) 2126-2132.

[33] R.A. Laskowski, J.A. Rullmannn, M.W. MacArthur, R. Kaptein, J.M. Thornton, AQUA and PROCHECK-NMR: programs for checking the quality of protein structures solved by NMR, J Biomol NMR, 8 (1996) 477-486.

[34] A.C. Wallace, R.A. Laskowski, J.M. Thornton, LIGPLOT: a program to generate schematic diagrams of protein-ligand interactions, Protein Eng, 8 (1995) 127-134.

[35] A.C. Barros, A.A. Takeda, T.R. Dreyer, A. Velazquez-Campoy, B. Kobe, M.R. Fontes, Structural and Calorimetric Studies Demonstrate that Xeroderma Pigmentosum Type G (XPG) Can Be Imported to the Nucleus by a Classical Nuclear Import Pathway via a Monopartite NLS Sequence, J Mol Biol, 428 (2016) 2120-2131.

[36] R.S. Sankhala, R.K. Lokareddy, G. Cingolani, Divergent Evolution of Nuclear Localization Signal Sequences in Herpesvirus Terminase Subunits, J Biol Chem, 291 (2016) 11420-11433.

[37] S. Vega, O. Abian, A. Velazquez-Campoy, On the link between conformational changes, ligand binding and heat capacity, Biochimica et biophysica acta, 1860 (2016) 868-878.

[38] Q. Ge, T. Nakagawa, R.M. Wynn, Y.M. Chook, B.C. Miller, K. Uyeda, Importin-alpha protein binding to a nuclear localization signal of carbohydrate response element-binding protein (ChREBP), J Biol Chem, 286 (2011) 28119-28127.

[39] L. Wirthmueller, C. Roth, G. Fabro, M.C. Caillaud, G. Rallapalli, S. Asai, J. Sklenar, A.M. Jones, M. Wiermer, J.D. Jones, M.J. Banfield, Probing formation of cargo/importin-alpha transport complexes in plant cells using a pathogen effector, Plant J, 81 (2015) 40-52.

[40] E. Conti, J. Kuriyan, Crystallographic analysis of the specific yet versatile recognition of distinct nuclear localization signals by karyopherin alpha, Structure, 8 (2000) 329-338.

[41] S.N. Yang, A.A. Takeda, M.R. Fontes, J.M. Harris, D.A. Jans, B. Kobe, Probing the specificity of binding to the major nuclear localization sequence-binding site of importin-alpha using oriented peptide library screening, J Biol Chem, 285 (2010) 19935-19946.

[42] A.C. de Barros, A.A. Takeda, C.W. Chang, B. Kobe, M.R. Fontes, Structural basis of nuclear import of flap endonuclease 1 (FEN1), Acta Crystallogr D Biol Crystallogr, 68 (2012) 743-750.

[43] B. Catimel, T. Teh, M.R. Fontes, I.G. Jennings, D.A. Jans, G.J. Howlett, E.C. Nice, B. Kobe, Biophysical characterization of interactions involving importin-alpha during nuclear import, J Biol Chem, 276 (2001) 34189-34198.

[44] M.L. Cutress, H.C. Whitaker, I.G. Mills, M. Stewart, D.E. Neal, Structural basis for the nuclear import of the human androgen receptor, J Cell Sci, 121 (2008) 957-968.

[45] K. Lott, A. Bhardwaj, P.J. Sims, G. Cingolani, A minimal nuclear localization signal (NLS) in human phospholipid scramblase 4 that binds only the minor NLS-binding site of importin alpha1, J Biol Chem, 286 (2011) 28160-28169.

[46] C.W. Chang, R.L. Counago, S.J. Williams, M. Boden, B. Kobe, Crystal structure of rice importin-alpha and structural basis of its interaction with plant-specific nuclear localization signals, Plant Cell, 24 (2012) 5074-5088.

[47] N.E. Bernardes, A.A. Takeda, T.R. Dreyer, F.Z. Freitas, M.C. Bertolini, M.R. Fontes, Structure of Importin-alpha from a Filamentous Fungus in Complex with a Classical Nuclear Localization Signal, PLoS One, 10 (2015) e0128687.

[48] S. Virgilio, F.B. Cupertino, N.E. Bernardes, F.Z. Freitas, A.A. Takeda, M.R. Fontes, M.C. Bertolini, Molecular Components of the Neurospora crassa pH Signaling Pathway and Their Regulation by pH and the PAC-3 Transcription Factor, PLoS One, 11 (2016) e0161659.

[49] J. Nardozzi, N. Wenta, N. Yasuhara, U. Vinkemeier, G. Cingolani, Molecular basis for the recognition of phosphorylated STAT1 by importin alpha5, J Mol Biol, 402 (2010) 83-100.

[50] H. Miyatake, A. Sanjoh, T. Murakami, H. Murakami, G. Matsuda, K. Hagiwara, M. Yokoyama, H. Sato, Y. Miyamoto, N. Dohmae, Y. Aida, Molecular Mechanism of HIV-1 Vpr for Binding to Importin-alpha, J Mol Biol, 428 (2016) 2744-2757.

[51] A. Giesecke, M. Stewart, Novel binding of the mitotic regulator TPX2 (target protein for Xenopus kinesin-like protein 2) to importin-alpha, J Biol Chem, 285 (2010) 17628-17635.

[52] R.D. Kolodner, G.T. Marsischky, Eukaryotic DNA mismatch repair, Curr Opin Genet Dev, 9 (1999) 89-96.

[53] N.O. Knudsen, F.C. Nielsen, L. Vinther, R. Bertelsen, S. Holten-Andersen, S.E. Liberti, R. Hofstra, K. Kooi, L.J. Rasmussen, Nuclear localization of human DNA mismatch repair protein exonuclease 1 (hEXO1), Nucleic Acids Res, 35 (2007) 2609-2619.

[54] A. Brieger, G. Plotz, S. Zeuzem, J. Trojan, Thymosin beta 4 expression and nuclear transport are regulated by hMLH1, Biochem Biophys Res Commun, 364 (2007) 731-736.

[55] R.C. Edgar, MUSCLE: multiple sequence alignment with high accuracy and high throughput, Nucleic acids research, 32 (2004) 1792-1797.

[56] M.H. Chen, I. Ben-Efraim, G. Mitrousis, N. Walker-Kopp, P.J. Sims, G. Cingolani, Phospholipid scramblase 1 contains a nonclassical nuclear localization signal with unique binding site in importin alpha, J Biol Chem, 280 (2005) 10599-10606.

TABLE LEGENDS

TABLE 1 - NLS peptides used for crystallization and isothermal titration calorimetry assays.

TABLE 2 - X-ray data collection and refinement statistics.

TABLE 3 - Binding parameters of Impα and NLS peptides by isothermal titration calorimetry assays.

TABLE 4 - Binding of monopartite NLSs to specific binding pockets of Impα.

FIGURE LEGENDS

Fig. 1. Crystal structure of the Impα-MLH1 NLS complex. (A) Overall structure of the Impα-MLH1 NLS complex. Impα is shown as a ribbon diagram and MLH1 NLS peptides at the major and minor binding sites are shown in stick representation. Electron density omit map of the MLH1 NLS peptide at the (B) major and (C) minor site regions of Impα (contoured at 3.0 s.d.). The main peptide residues are labeled in their corresponding binding position. The main peptide residues from (D) major and (E) minor binding sites of Impα are identified in colored scheme (Trp - green, Asn - purple, glutamic and aspartic acids- red).

Fig. 2. Crystal structure of the Impα-PMS2 NLS complex. (A) Overall structure of the Impα-PMS2 NLS complex. Impα is shown as a ribbon diagram and the PMS2 NLS peptide at the major and minor binding sites are shown in stick representation. (B) Electron density omit map of the PMS2 NLS peptide at the major site region of Impα (contoured at 3.0 s.d.). (C) The main peptide residues from major binding site of Impα are identified in colored scheme (Trp - green, Asn - purple, glutamic and aspartic acids- red).

Fig 3. Schematic diagram of the interactions between the MLH1 and PMS2 NLS peptides and the minor and major binding sites of Impα. The peptide backbone is drawn in salmon (A, MLH1 NLS) or cyan (B, PMS2 NLS) with the residues identified by one letter code. Impα side-chain residues interacting with the peptide are indicated with their names and different colors. Polar contacts are shown with dashed lines, and hydrophobic contacts are indicated by arcs with radiating spokes.

Fig 4. Calorimetric titration of SV40TAg, PMS2, MLH1 and PMS2L NLS peptides with Impα. The upper panel shows the raw data thermogram (thermal power as a function of time) of the titration of Impα with (A) SV40TAg NLS, (B) PMS2 NLS, (C) MLH1 NLS and (D) PMS2L NLS. The lower panel shows the binding isotherm (ligand-normalized integrated heat as a function of the molar ratio). Titrations were performed at least in duplicate in 20 mM TrisHCl, 100 mM NaCl buffer (pH 8.0) at 20 °C.

SUPPLEMENTARY FIGURE LEGENDS

Suppl. Fig 1. Sequence alignment between Importin-α (Gene KPNA2). Importin-α protein sequences from *Mus musculus* (MmImpα) and *Homo sapiens* (MmImpα) (NCBI reference sequences: NP_034785.1and NP_002257.1, respectively) were aligned in MUSCLE software [55]. The highlighted residues correspond to the essential residues in NLS recognition by Impα [14], which indicates residues from the major binding site (orange), a residue in the linker region (grey) and the minor binding site (light blue).

Suppl. Fig 2. Comparison of NLS peptides in the minor and major NLS binding sites. NLSs from MLH1 (rose), PMS2 (blue), XPG1 (purple) [34], XPG2 (orange) [34], SV40TAg (green) [29], Ku70 (orange) [23] and Ku80 (yellow) [23] are superimposed. Positions binding to the major (P_1-P_5) and minor binding sites ($P_1^{'}$-$P_4^{'}$) are identified along the chains.

Suppl. Fig 3. Calorimetric titration of MLH1L NLS peptides with Impα. Titrations were performed at least in duplicate in 20 mM TrisHCl, 100 mM NaCl buffer (pH 8.0) at 20 and 10 °C, A and B respectively. The upper panel shows the raw data thermogram (thermal power as a function of time) of the titration of Impα with MLH1L NLS. The lower panel shows the binding isotherm (ligand-normalized integrated heat as a function of the molar ratio).

TABLE 1. NLS peptides used for crystallization and isothermal titration calorimetry assays.

Protein	NLS
MLH1[*]	[466]SSNPRKRHRED[476]
MLH1 K471N[**]	[466]SSNPRNRHRED[476]
MLH1 R472N[**]	[466]SSNPRKNHRED[476]
PMS2[*]	[571]LATPNTKRFKKEE[583]
PMS2 K577N[**]	[571]LATPNTNRFKKEE[583]
PMS2 R578N[**]	[571]LATPNTKNFKKEE[583]
MLH1L[***]	[459]SEKRGPTSSNPRKRHRED[476]
PMS2L[***]	[625]LAKRIKQL[632]

[*][4]; [**][3]; [***][24]

TABLE 2
X-ray data collection and refinement statistics

Diffraction data statistics	MLH1 NLS-Impα	PMS2 NLS-Impα
Unit cell dimensions (Å)	a=77.21, b=89.07, c=99.14	a=77.14, b=89.54, c=97.03
Space group	P2₁2₁2₁	
Resolution (Å)	40.0-2.17 (2.25-2.17)[a]	40.0-2.10 (2.18-2.10)[a]
Unique reflections	36,607	39,804
Multiplicity	6.4 (5.4)[a]	2.9 (2.6)[a]
Completeness (%)	99.5 (97.9)[a]	99.7 (98.9)[a]
R_{merge}[b] (%)	7.4 (61.8)[a]	6.1 (46.8)[a]
Average $I/\sigma(I)$	24.11 (2.4)[a]	18.56 (2.2)[a]
Refinement statistics		
Resolution (Å)	40.0-2.17 (2.25-2.17)[a]	40.0-2.10 (2.18-2.10)[a]
Number of reflections	36,590	39,795
R_{cryst} (%)[c]	18.1	17.3
R_{free} (%)[d]	21.0	20.7
Number of non-hydrogen atoms:		
Protein	3,247	3,217
Peptide	164	89
Solvent	225	332
Mean B-factor (Å²)	45.2	47.9
Coordinate error (Å)[e]	0.21	0.24
R.m.s deviations from ideal values[e]:		
Bond lengths (Å)	0.008	0.008
Bond angles (°)	1.03	0.95
Ramachandran plot:		
Residues in most favored (disallowed) regions (%)[f]	98.0 (0.4)	99.0 (0.0)

[a] Values in parentheses are for the highest-resolution shell.
[b] Rmerge=Σhkl(Σi(|Ihkl,i−⟨Ihkl⟩|))/Σhkl,i⟨Ihkl⟩, where Ihkl,i is the intensity of an individual measurement of the reflection with Miller indices h, k and l, and ⟨Ihkl⟩is the mean intensity of that reflection. Calculated for I>−3 σ(I) [28].
[c] Rcryst=Σhkl(||Fobs,hkl|−|Fcalc,hkl||)/|Fobs,hkl|,where |Fobs,hkl|and |Fcalc,hkl| are the observed and calculated structure factor amplitudes, respectively.
[d] Rfree is equivalent to Rcryst but calculated with reflections (5%) omitted from the refinement process.
[e] Calculated based on Luzzati plot with the program SFCHECK [33].
[f] Calculated with the program PROCHECK [33].

Table 3. Binding parameters of Impα with NLS peptides determined by ITC

| NLS-peptides		Major binding site	Minor binding site
PMS2	K_d (μM)	1.94±0.21	
	ΔH (kcal/mol)	-5.21±0.10	
PMS2-K577N	K_d (μM)	No binding	
	ΔH (kcal/mol)		
PMS2-R578N	K_d (μM)	No binding	
	ΔH (kcal/mol)		
MLH1	K_d (μM)	0.10±0.02	1.5±0.2
	ΔH (kcal/mol)	-6.5±0.7	-2.9±0.7
MLH1-K471N	K_d (μM)	No binding	
	ΔH (kcal/mol)		
MLH1-R472N	K_d (μM)	No binding	
	ΔH (kcal/mol)		
SV40 TAg	K_d (μM)	1.8±0.4	23±5
	ΔH (kcal/mol)	-9.5±0.6	4.5±0.7
XPG1	K_d (μM)	0.45±0.05	3.4±0.5
	ΔH (kcal/mol)	-3.2±0.3	3.8±0.3
XPG2	K_d (μM)	0.91±0.09	140±20
	ΔH (kcal/mol)	-6.9±0.8	-21±1
PMS2L	K_d (μM)	0.39±0.09	6.54±1.2
	ΔH (kcal/mol)	-2.36±0.08	-0.56±0.04
MLH1L	K_d (μM)	No binding	
	ΔH (kcal/mol)		

SV40 TAg [14]; XPG1 and XPG2 [35] NLSs. No binding - No detectable binding.

**Table 4. Binding of monopartite NLSs to specific binding pockets of importin-α.**

| Proteins	Minor site S_2 (P0' P1' P2' P3' P4')	Major site S_1 (Linker X_{10-12} … P1 P2 P3 P4 P5)
SV40 TAg	P K **K** **K** R K V	A A P P K **K** **K** R **K** V E
CN-SV40	K **R** K V	… A P P K **K** **K** R **K** V
c-Myc	**K** **R** V K L	P A A **K** **R** V **K** L D
mPet TM	K **K** **R** R E A	F **K** **K** K **R** R E A
MLH1	S N P R **K** **R** H R E	S N P R **K** **R** H **R** E D
pUL15	P P **K** **K** R A	G P P K **K** **R** A **K** V D
pUL56	T R **K** **R** P R	A T R **K** **R** P **R** R A
XPG1	S L **K** **R** K R	S L **K** **R** K **R**
XPG2	R **K** **R** K T R	G K **K** **R** K L R
Ku80		… D G P T A **K** **K** L **K** T E
Ku70		… N E G S G S **K** **R** P **K**
PLSCR1		G **K** **I** S **K** H W
PLSCR4	S I **I** **R** K W N	
AR		E A G M T L G A R **K** **L** K **K** L G
PMS2		T P N T **K** **R** F **K** K E E
Consensus	**K R**	X_{10-12} **K**, **R/K**, **X**, **R/K**

SV40 TAg [14]; CN-SV40 [29]; c-Myc [40]; mPet TM [41]; pUL15 and pUL56 [36]; XPG1 and XPG2 [35]; Ku80 and Ku70 [23]; PLSCR1 [56]; PLSCR4 [45]; AR [44]. Consensus [15]. The positions highlighted in red correspond to the consensus NLS. The boldface positions correspond to exceptions to the consensus NLS.
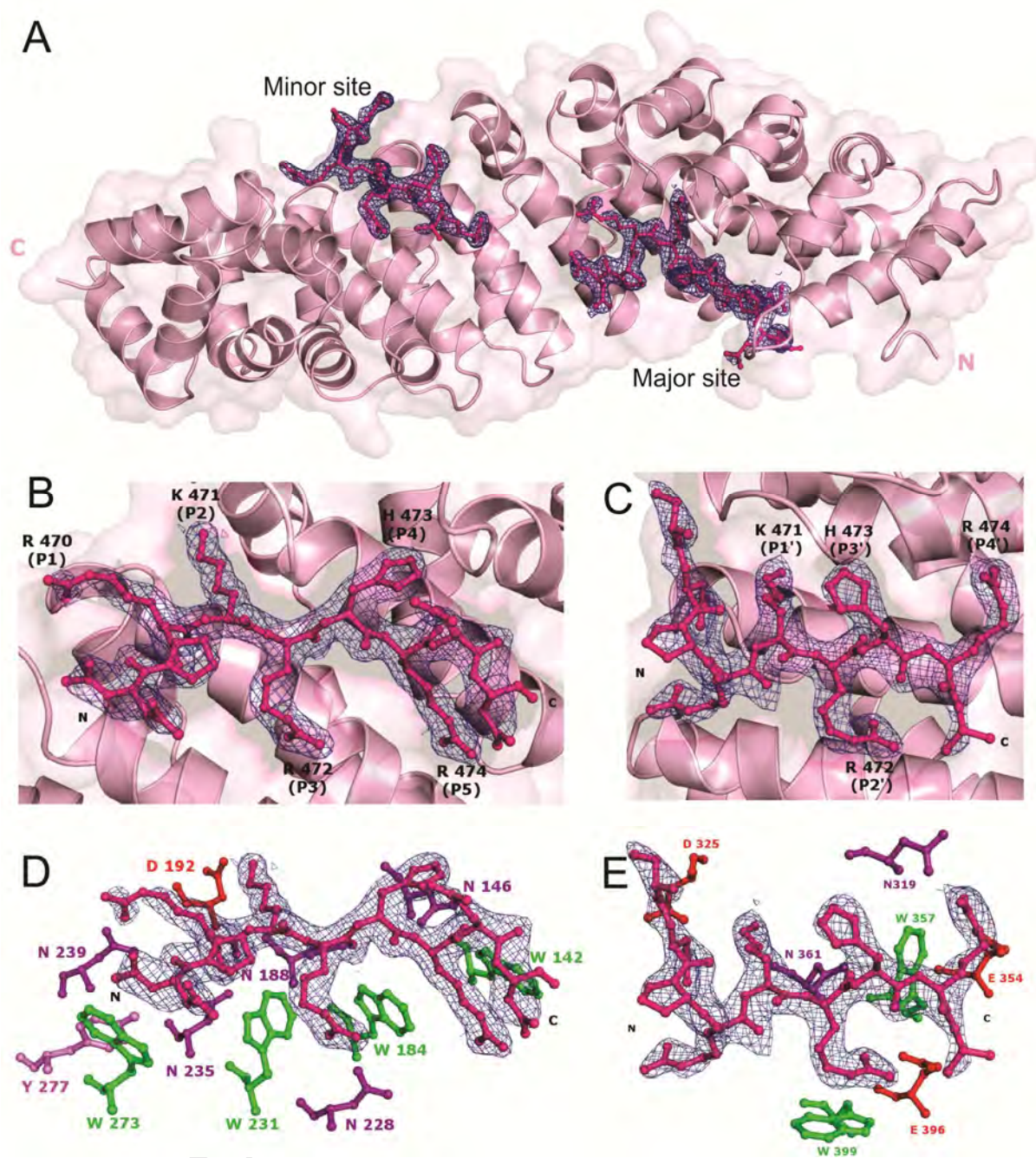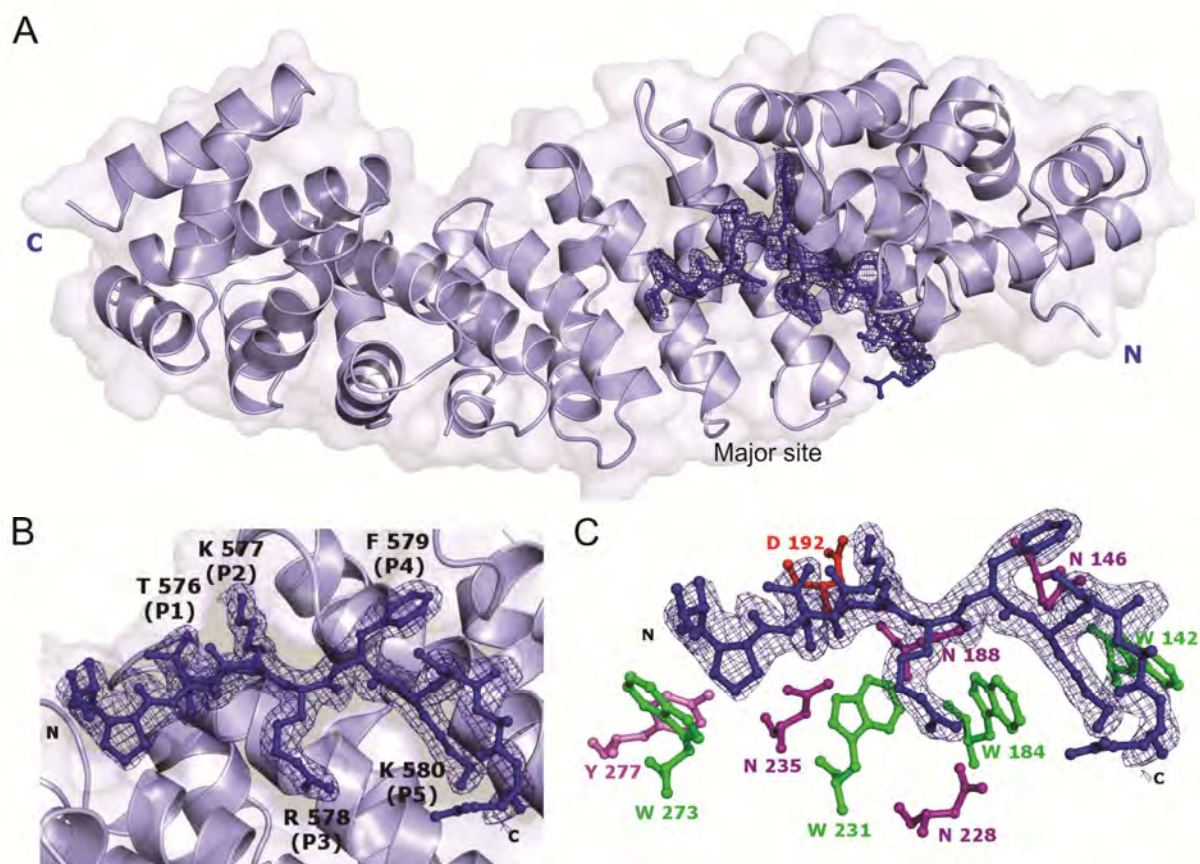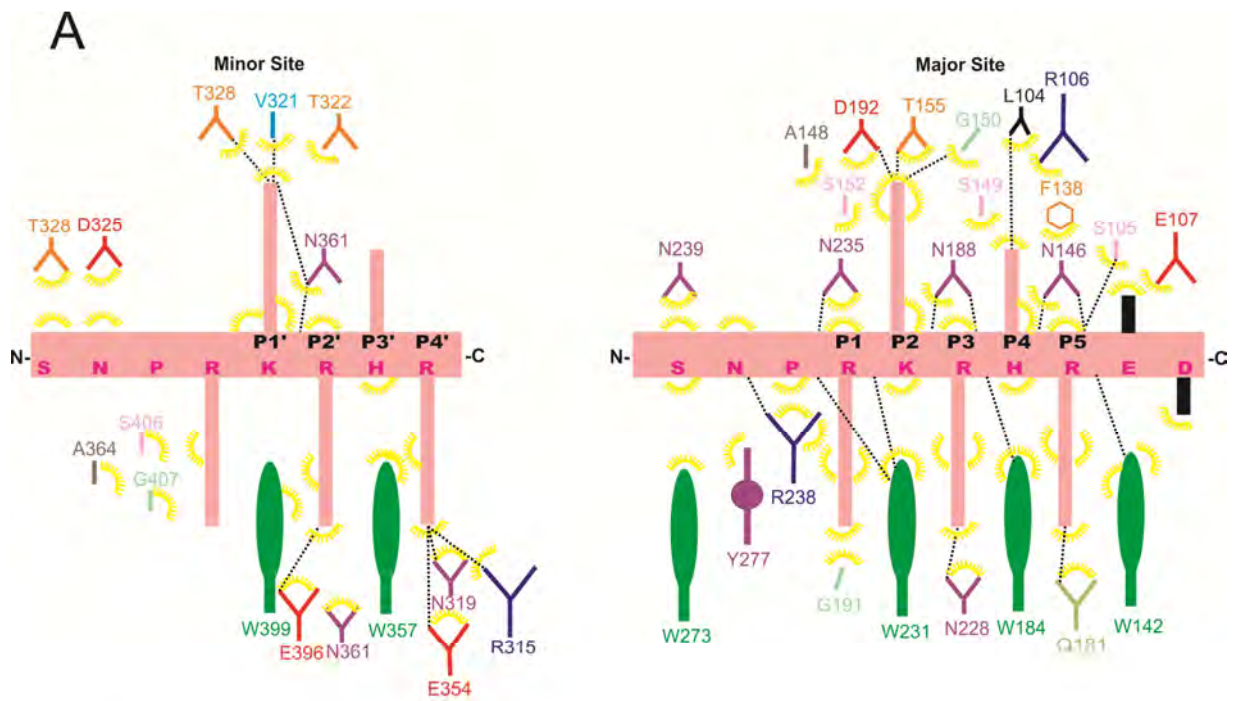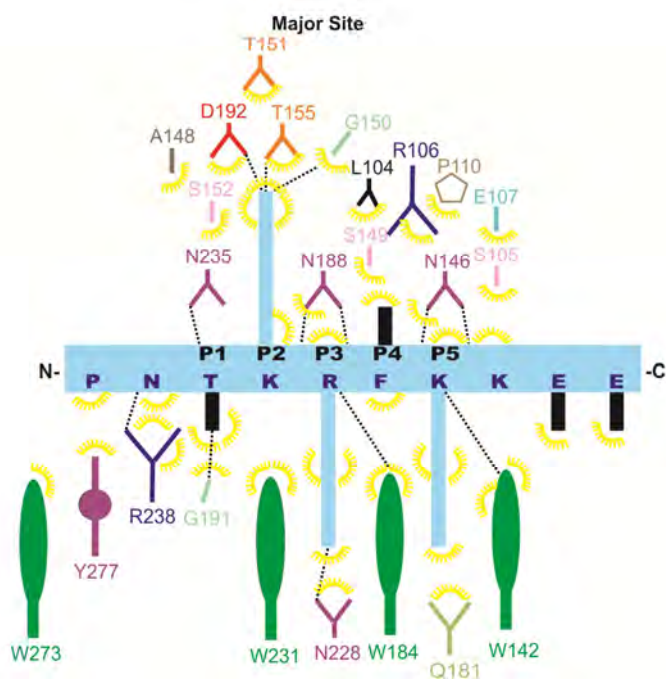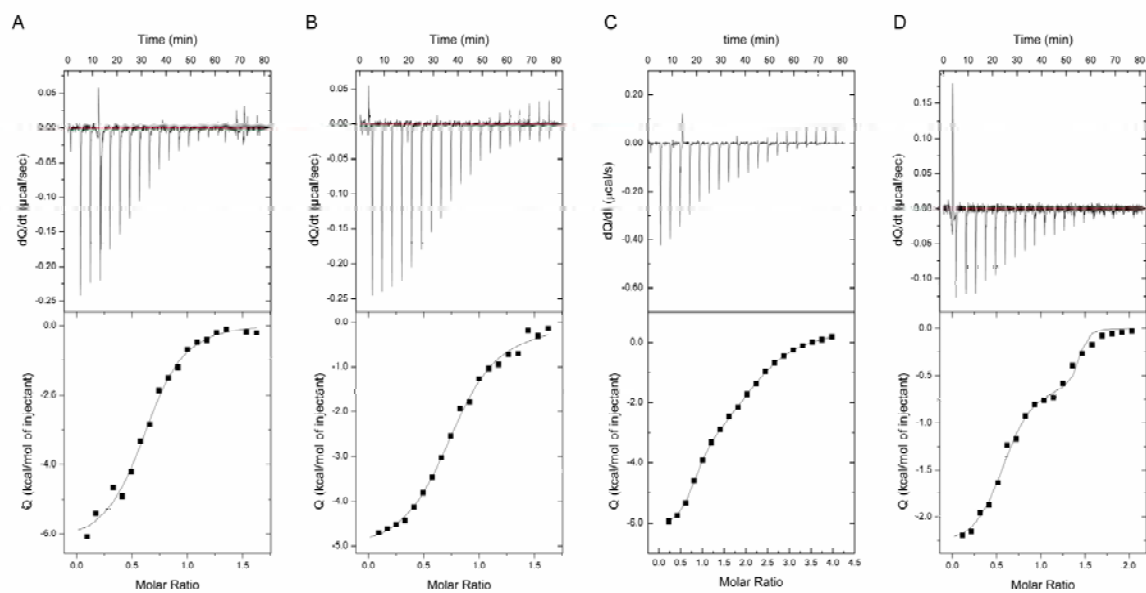
Structures of Importin-α and NLS peptides of MLH1 and PMS2 proteins were solved.

ITC assays with native and mutated MLH1 and PMS2 NLSs and Importin-α were performed.

Both putative peptides bind to Importin-α as monopartite NLSs.

MLH1 NLS present the highest affinity already measured for a natural NLS.

MLH1 NLS may have a major role in the MutLα heterodimer nuclear transport.